

Strong Anisotropy of Multilayer γ -InSe-Enabled Polarization Division Multiplexing Photodetection

Xusheng Wang, Bo Wen, Siyan Gao, Xiaolin Li, Zezhou Lin, Luping Du, and Xi Zhang*

Polarized light detection is consequential for optical communication and polarized light imaging. InSe is considered a promising candidate for narrow-bandgap photodetector. However, monolayer γ -InSe is an indirect bandgap semiconductor and is ignored for a long time for polarized light detection. In this work, by virtue of the indirect-direct conversation and the surface-bound excitons, the intrinsic anisotropy of multilayer γ -InSe is revealed by the photoluminescence (PL) measurement under polarized light. Due to the anisotropy of surface-bound exaction and in-plane exciton, there are significant differences in the photocurrent under irradiation of laser with different polarization angles. The γ -InSe-based photodetector exhibits considerable polarization-dependent photocurrent with an outstanding anisotropic ratio of 2.7. Moreover, the multilayer γ -InSe photodetector shows high responsivity of 7.47 A W^{-1} and specific detectivity of 4.56×10^{13} Jones under 785 nm laser. Based on the InSe polarization photodetector, a polarization division multiplexing that can simultaneously process four information tracks and enhance the communication speed by 2^4 is explored. The multilayer InSe polarization photodetector proposed in this work broadens a new path for polarized light detection, and brings a potential solution to the field of optical communications.

1. Introduction

In the past decades, polarization photodetectors had attracted a lot of attention for their immense potential in remote sensing imaging, environment monitoring, optical navigation, and communication.^[1–9] However, the actual needs are still difficult to meet, academics and engineers are still committing to achieve excellent performance in polarized light detection. Since the successful preparation of graphene, photodetectors based on 2D semiconductor materials became the pivot of photoelectric research, and the 2D semiconductor materials are considered to be the most suitable candidates for polarization photodetectors because of their unique structural properties and photoelectric performance.^[10–14] Owing to the advantages of high mobility, direct bandgap, and linear dichroism,^[9,15–17] 2D black phosphorus polarization photodetectors show considerable photoresponsivity and response speed. However, 2D black phosphorus is extremely unstable in the


atmosphere and the approaches of protection remain to be studied, which limits the applications in polarization detecting.^[18–21] Transition metal dichalcogenides (TMDs) such as MoS_2 , MoSe_2 , and ReS_2 are other kinds of materials commonly used for photodetectors because of their photoelectric properties and intrinsic anisotropy.^[22–26] Although polarization photodetectors based on TMDs showed high photoresponsivity, they had the problems of slow photoresponse and low absorbance.^[27–29]

Recently, 2D III–VI group chalcogenides exhibit an obvious in-plane anisotropy behavior in carrier transport, thermal conductivity, electrical conductivity, thermoelectric transport, and optical absorption processes, and have attracted enormous attention. Among all of them, indium selenide (InSe) exhibits not only ultrahigh carrier mobility and narrow bandgap, but also high absorbance properties.^[30–36] The indirect-to-direct bandgap, excitons, and optoelectronic properties of 2D InSe have been reported recently.^[37,38] Therefore, InSe-based photodetectors are a promising candidate for a narrow-bandgap photodetector.^[39,40] However, monolayer γ -InSe is an indirect bandgap semiconductor and was ignored for a long time for polarized light detection.^[41,42] It is still a challenge to fabricate high-performance InSe polarization photodetectors adapting with actual working conditions.

X. Wang, B. Wen, S. Gao, X. Li, X. Zhang
Institute of Nanosurface Science and Engineering
Guangdong Provincial Key Laboratory of Micro/Nano Optomechatronics Engineering
Shenzhen University
Shenzhen 518060, China
E-mail: zh0005xi@szu.edu.cn

Z. Lin
Department of Applied Physics and Research Institute for Smart Energy
The Hong Kong Polytechnic University
Hong Kong SAR 999077, China

L. Du
Nanophotonics Research Centre
Institute of Microscale Optoelectronics
Shenzhen University
Shenzhen 518060, China

 The ORCID identification number(s) for the author(s) of this article can be found under <https://doi.org/10.1002/adpr.202200119>.

© 2022 The Authors. Advanced Photonics Research published by Wiley-VCH GmbH. This is an open access article under the terms of the Creative Commons Attribution License, which permits use, distribution and reproduction in any medium, provided the original work is properly cited.

DOI: 10.1002/adpr.202200119

Here in this work, we propose an impressively sensitive polarization photodetector based on multilayer γ -InSe. By virtue of the indirect-direct conversion and the surface-bound excitons, the intrinsic anisotropy of multilayer γ -InSe is revealed by the photoluminescence (PL) measurement under polarized light. The measured photoelectric responsivity and response time excited with a 785 nm laser shows the high performance of the γ -InSe-based photodetector. Benefitting from the ultrahigh mobility of multilayer InSe, this device has a remarkable response time and decay time of 27 μ s. The γ -InSe-based photodetector exhibits considerable polarization-dependent photocurrent with an outstanding anisotropic ratio of 2.7. Based on the InSe polarization photodetector, we explored a polarization division multiplexing (PDM), which can simultaneously process four information tracks and enhance the communication speed by 2^4 . Within this study, a sensitive polarization photodetector with outstanding photoelectric performance based on multilayer γ -InSe is investigated, and it is expected to pay the way for precise polarization imaging and navigation.

2. Results and Discussions

Figure 1a shows the side view and top view of the crystal structure of InSe. The photodetector is prepared by dry transferring a multilayer InSe sheet onto the SiO_2/Si substrate. Then, Ti/Au electrodes were patterned by conventional photolithography, metal deposition, and lift-off processes. A single layer of InSe is composed of four bonded Se–In–In–Se atomic planes, while several layers of InSe are vertically stacked into bulk γ -InSe crystal with a slight shift. Due to the weak van der Waals force between the InSe layers, the multilayer InSe can be prepared by mechanical exfoliation. As shown in the top view, the electrons transported along the armchair and zigzag direction exhibit anisotropy.^[43] The orbit of electrons along the armchair direction is discontinuous because of the honeycomb cavity, which means it has a higher potential barrier and makes it difficult for electrons transporting. On the contrary, the potential barrier of electrons along the zigzag direction is smaller, it is more conducive to the transmission of electrons.

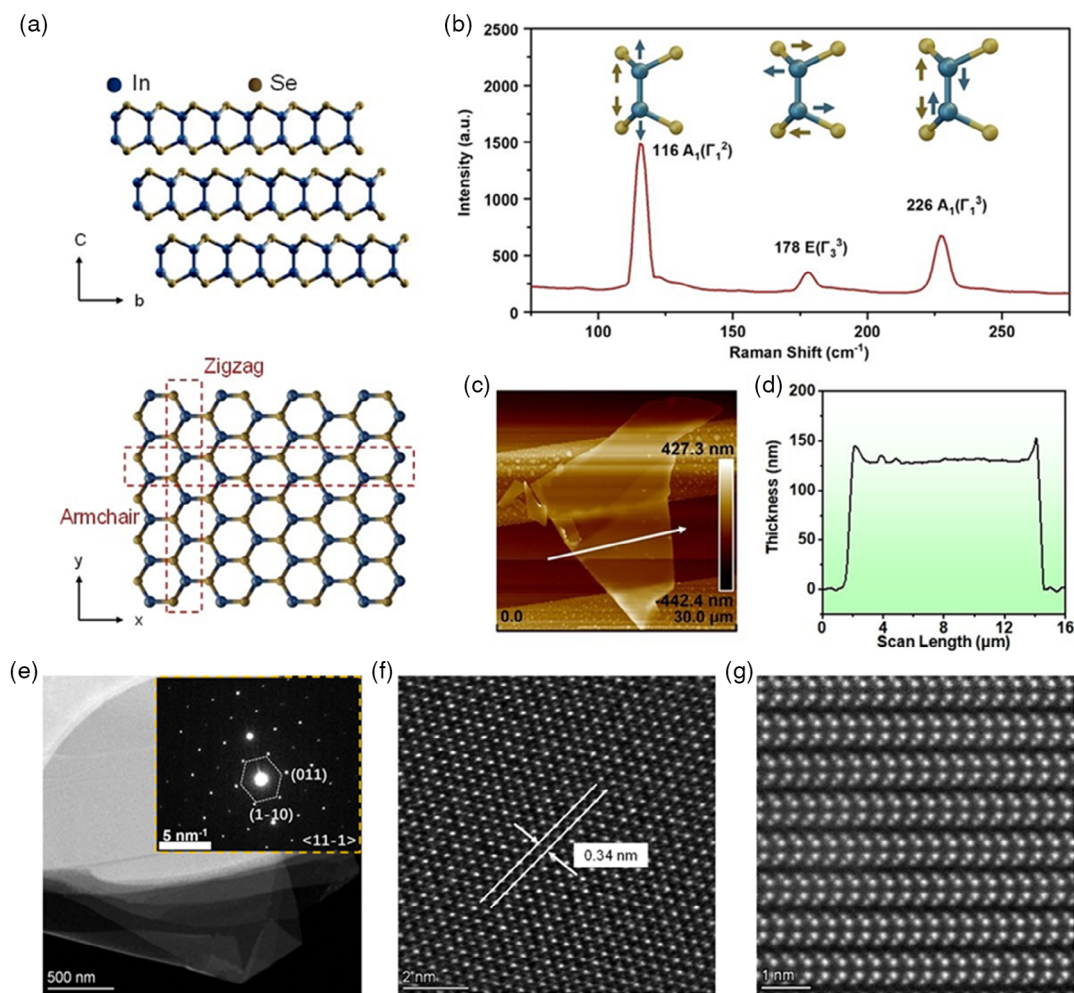


Figure 1. a) Side view and top view of the crystal structure of InSe, where the blue and yellow dots represent the indium and selenium atom, respectively. b) Raman spectrum of the prepared sample, which shows the three vibration modes of multilayer γ -InSe. c) Atomic force microscopy (AFM) image of multilayer InSe photodetector, which shows a neat and uniform topography. d) Thickness of multilayer γ -InSe along the marked direction measured by step profiler, which shows the smooth surface of the photodetector. e) Low-resolution transmission electron microscope (TEM) plane image, the in-chart shows the selected area electron diffraction pattern of InSe. f) High-resolution TEM plane-view image. g) High-resolution TEM cross-section image.

Here in this study, the γ -InSe crystal is prepared by the Bridgman method, and the high-quality multilayer sheets are prepared by mechanical exfoliation. As shown in Figure 1b, the Raman spectrum of the prepared sample is measured to verify its phase. It can be seen that three peaks show at 116, 178, and 227 cm^{-1} , which are attributed to A_{1g}^1 , E_{2g}^1 , and A_{2g}^1 . The Raman results are consistent with the vibration modes of γ -InSe, which proves that the as-prepared samples are γ -InSe sheets. What's more, a thickness-dependent Raman spectrum of the γ -InSe film with different layers is also obtained (See Figure S1, Supporting Information), it can be seen from the measurements that the Raman intensity is higher with the increase of film thickness, which is consistent to the previous study.^[44] As shown in Figure 1c, an atomic force microscopy (AFM) image is used to determine the fabrication quality of this photodetector. It can be seen that multilayer γ -InSe has a neat surface and hardly has defects, which is a benefit to the photoelectric response. Furthermore, the thickness of multilayer InSe is measured, as shown in Figure 1d. Along the selected direction, the thickness of the InSe nanofilm is around $129\text{ }\mu\text{m}$, indicating the smooth surface and proving that this samples have a multilayer structure. Figure 1e-g shows the transmission electron microscope (TEM) images. The plane view TEM image of the sample shows a lattice distance of 0.34 nm , which is corresponding to the γ -InSe. As the cross-section TEM image shows, each layer of InSe shows a certain shift while stacking, which further indicates that the sample is multilayer γ -InSe. There are certain differences in atomic orbits along the armchair and zigzag directions, which makes γ -InSe anisotropy.

To study the anisotropy of multilayer γ -InSe, it is necessary to understand how the electrons transit in multilayer InSe.

Therefore, the PL spectrum of multilayer γ -InSe under polarized light is measured. The schematic diagram of the optical measurement system is shown in Figure 2a. At room temperature, a 588 nm laser is used as a light source. By rotating the $1/2$ waveplate, the linear polarization angle of the laser is changed and it is vertically irradiating to the multilayer γ -InSe. Through the focus of the objective lens, the light spot on the sample can be reduced to around $1\text{ }\mu\text{m}$. The PL signal of multilayer InSe is analyzed by the spectrometer and the photoelectric signal can be obtained by the semiconductor film analyzer. Since the wavelength range of multilayer InSe photoluminescence is between 800 and 1100 nm , a filter with a wavelength of $780\text{--}1100\text{ nm}$ is used to filter the original laser signal. The schematic diagram of the multilayer γ -InSe polarization photodetector is shown in Figure 2b. Unlike atomic layers InSe which has an indirect bandgap, multilayer γ -InSe has a direct bandgap so that the electrons can easily transit between the conduction band and valence band which can induce high PL intensity.^[45] When the laser is irradiating, the electrons are excited from the valence band to the conduction band, then, photo-generated electrons transit back to the valence band and then re-emit photons. By analyzing the PL intensities under different polarization angles, the intrinsic anisotropy of InSe can be confirmed. Under the irradiation of 588 nm laser, the emission wavelength of multilayer indium selenide is 984 nm . As shown in Figure 2c, when the laser polarization angle changes from 0 to 90° , multilayer γ -InSe show obvious emission peaks. The main emission peaks are located at 1.26 eV , which corresponds to the transition from the first valence band maximum to the conduction band minimum.^[46] Since the multilayer γ -InSe has a direct band gap, the recombination of electrons and holes is more intense, resulting in great PL intensity.

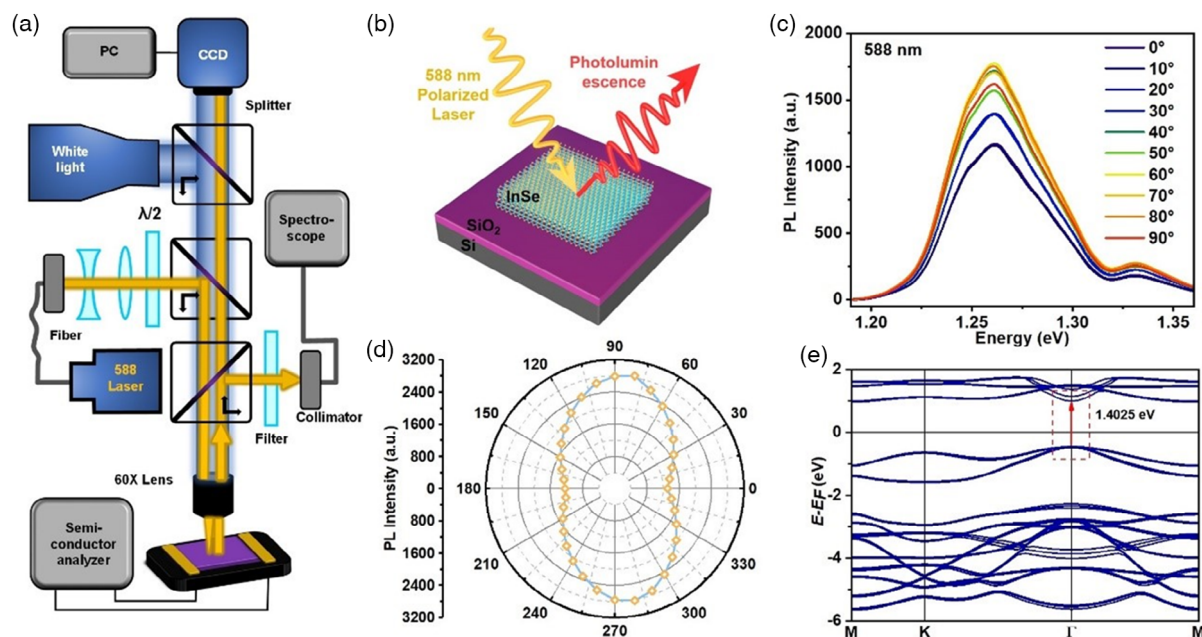


Figure 2. a) Schematic diagram of the optical path of the test system and the schematic diagram of multilayer InSe, photoluminescence (PL) signals are detected by the spectrometer, and the photocurrent signals are analyzed by the semiconductor film analyzer. b) Schematic diagram of PL phenomenon of multilayer InSe. c) PL spectrum of multilayer γ -InSe as a function of polarization angles. d) Polar plot of PL intensity at 1.26 eV under various polarization angles. e) Band structure diagram of multilayer γ -InSe.

Furthermore, the location of the main emission peak indicates that the as-prepared sample is multilayered γ -InSe, it also proves that the samples prepared by mechanical exfoliation exhibit high quality and hardly had no inner strain.^[45] As polarization angles increase from 0 to 90°, the PL intensity prominently increases from 1168 to 1789, and the anisotropic ratio of PL intensity can be calculated by $PL_{90^\circ}/PL_{0^\circ} \approx 1.53$. It can be seen that the PL intensity of multilayer InSe is very sensitive to polarized light, indicating the great anisotropy in the recombination rate between electrons and holes in InSe under different polarization angles.

Furthermore, we studied the change of PL intensity at 1.26 eV with the periodic change of polarized light. As shown in Figure 2d, the PL intensities at 1.26 eV of one cycle of polarization angles show two obvious peaks and valleys, with a stable periodic of 180°. On the one hand, the period of PL intensity varying with polarization angle is the same as the included angle between the armchair and zigzag directions in γ -InSe. On the other hand, it can be seen that the peak and valley values of PL intensity remain stable in every cycle, and the trends remain the same, which corresponds to the symmetrical crystal structure of γ -InSe. Obviously, the polarization sensitivity of multilayer γ -InSe is mainly attributed to the intrinsic anisotropy of crystal structure, resulting in great differences in electrons transition at different polarization angles. To understand the principle of polarization-dependent change of PL intensity, the band-structure diagram is obtained by density functional theory (DFT) calculation, which is shown in Figure 2e and the corresponding schematic diagram of the Brillouin zone is shown in Figure S2, Supporting Information. The bandgap between the conduction band and valence band at Γ point is 1.4025 eV, and the band structure of Γ to K and Γ to M range represents the electrons' transition along zigzag and armchair directions, respectively. As marked in the red rectangle, the conduction band structures in these two directions show asymmetry at the Γ point. Moreover, since the band curvature is a key parameter that affects the electron transition rate, the electron transition rate along the armchair and zigzag directions in γ -InSe is strongly anisotropic. Recently, we showed that InSe contained the surface-bound excitons and in-plane excitons which can show strong optical anisotropy (See Figure S3, Supporting Information). Therefore, the electron transition rate of multilayer γ -InSe will change along with the polarization angle. When the polarization angle is along the armchair direction, the electron transition rate is the smallest, so the PL intensity is the smallest. On the contrary, when the polarization angle is along the zigzag direction, the PL intensity of γ -InSe reaches the maximum.

Figure 3a,b shows a schematic diagram of the multilayer γ -InSe polarized photodetector and the band alignment between multilayer InSe and the Au electrodes, respectively. In the process of device fabrication, the contact between Au and multilayer indium selenide makes the energy band of InSe bend, and a Schottky contact is formed, where Φ_{SB} represents the height of the Schottky barrier. Since the work function of gold (5.1 eV) is greater than the electron affinity of InSe (4.05 eV), the energy band of InSe bends upward, and the Φ_{SB} is reached up to 1.05 eV. Due to the large Schottky barrier, electrons can flow from InSe to Au, thereby forming a built-in electric field at the interface, which in turn inhibits the free movement of

electrons and effectively reduces the noise. Under light irradiation, the electrons in the valence band absorb the energy of photons and transit to the conduction band, with the external bias, the photoexcited electrons are attracted and move toward the positive electrode, while the holes move in the opposite direction, forming a significant photocurrent.

As an excellent photodetector, it is indispensable to have technical advantages such as high responsivity and fast photoelectric response. To determine the performance of the multilayer InSe photodetector, we used a laser with a wavelength of 785 nm and a power from 0.1 to 110 mW to irradiate the device. The I - V curves of this photodetector are shown in Figure 3c, lines of different colors represent I - V curves at different laser power and dark environment. While working in a dark environment, this device shows a low dark current (I_{dark}) of around nanoampere level as a result of the large Φ_{SB} . When laser irradiates to the photodetector, the electron-hole pairs in multilayer InSe appear and the movement of photoexcited electrons generates considerable photoresponse. At zero bias, the illumination current ($I_{illumination}$) of the multilayer InSe photodetector increase from picoampere level (156.96 pA) to nanoampere level (188.22 nA) when the laser power increase from 0.1 to 110 mW, which is attributed to the increasing number of photoexcited electrons under high power laser. Then, biases from -5 to 5 V with an interval of 0.1 V are applied. Under the attraction of an external electric field, the electron-hole pairs will separate rapidly, and the recombination rate will decrease accordingly, resulting in a higher photocurrent. When $V_{sd} = -5$ V, $I_{illumination}$ of multilayer InSe photodetector increase from nanoampere level (105.08 nA) to microampere level (1.98 μ A) when the laser power increase from 0.1 to 110 mW. Additionally, the value of $I_{illumination}$ also shows an excellent linear relationship with the bias voltage. Under 110 mW laser, as V_{sd} raise from 0 to -4 V, the $I_{illumination}$ increase from to, but the increasing trend of $I_{illumination}$ decrease as V_{sd} increase from -4 to -5 V. Although the V_{sd} is increasing, the number of photogenerated electrons is limited under a certain laser power. With the advantage of high photoelectric response, the use of complex signal processing circuits would be unnecessary, making multilayer InSe photodetector more potential in practical applications.

The polarized light detection performance of this device is studied by measuring polarization-dependent photocurrent. The 785 nm linear polarized laser perpendicularly irradiates to the photodetector, while the photodetector is fixed to the probe station, which makes sure the change of photocurrent is attributed to the polarization angles instead of the horizontal angle between the laser and the photodetector. The polar plot of polarization-dependent photocurrent is shown in Figure 3d, in a single cycle of changing polarization angles, two peaks and valleys of photocurrent appear. It can be seen that the period of polarization-dependent photocurrent is found to be consistent with the PL spectrum, which once again proved the anisotropy of electronic transitions.^[43] The photocurrent shows the minimum of 0.1007μ A at 0° (armchair direction), and gradually increases to the maximum of 0.2709μ A as the polarization angle increases to 90° (zigzag direction). When the polarization angle is 90° , the laser is along the zigzag direction, which results in the largest number of photoexcited electrons and the photocurrent reaches the maximum. As the polarization angle increases to

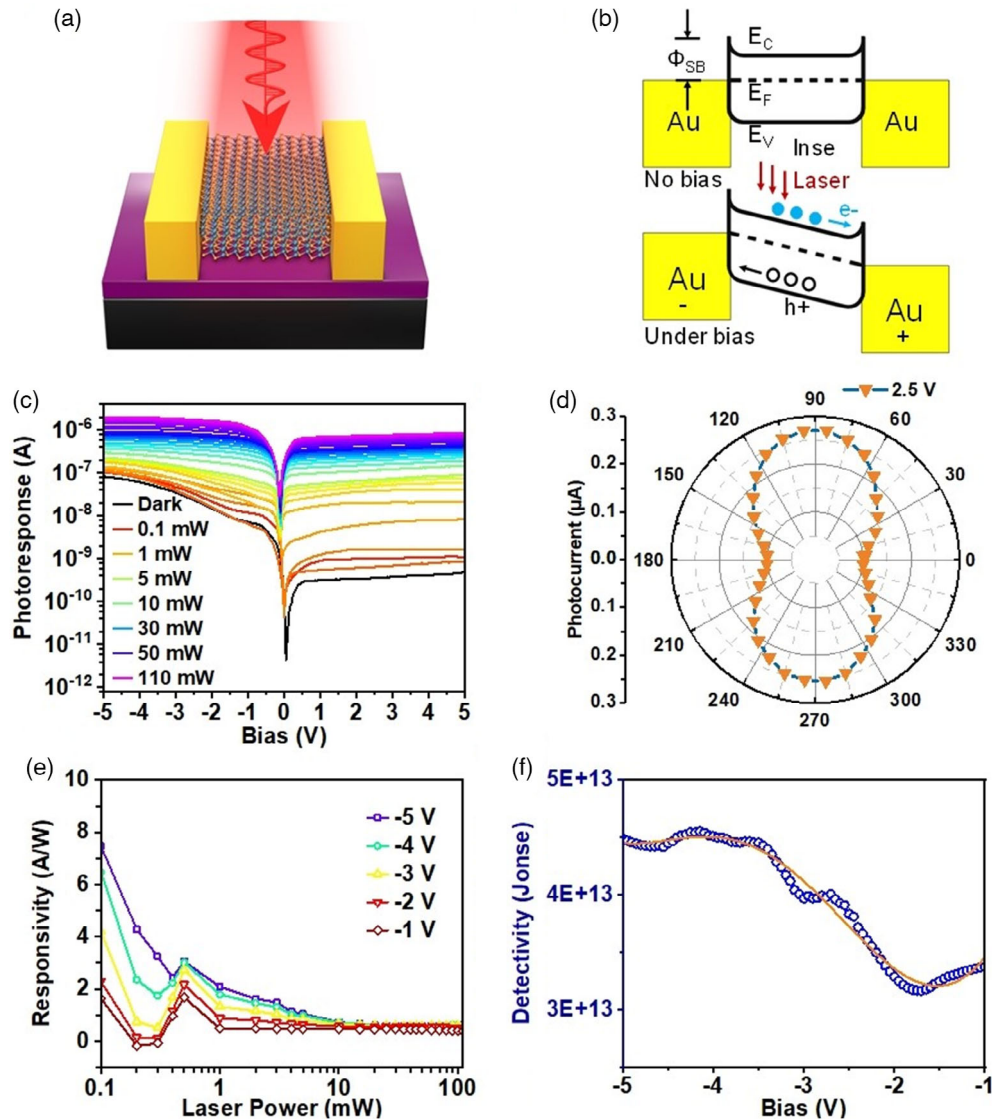


Figure 3. a) Schematic diagram of multilayer γ -InSe polarized photodetector. b) Band bending diagram of multilayer γ -InSe photodetector. c) Photocurrent-voltage (I_{ph} - V_{sd}) curves of multilayer γ -InSe photodetectors at the bias of from -5 to 5 V under 785 nm laser with different power. d) Polar plot of polarization dependence of the photocurrent at 2.5 V bias, with the laser power of 0.1 mW. e) Photoelectric responsivity curves of multilayer γ -InSe photodetectors at the bias of from -1 to -5 V while laser power increase from 0.1 to 110 mW. f) Specific detectivity under irradiation of 0.1 mW laser at different bias.

180° , the polarized light irradiates along the armchair direction. Therefore, the electrons transition rate is the lowest, which causes the minimum photocurrent value. The anisotropic ratio of polarization-dependent photocurrent was calculated as $I_{90^\circ}/I_{0^\circ} \approx 2.7$. The high anisotropic ratio of this photodetector is greater than some of the polarization photodetectors that are based on TMDs and III-VI group compounds,^[24,47–49] which indicates that the outstanding polarization detection ability of multilayer InSe polarization photodetector.

Responsivity (R) is a key parameter that reveals the photoelectric conversion ability, it is defined by the photocurrent produced by the device under the light irradiation of unit power. Here in this study, the R of multilayer InSe photodetector is given by

$$R = \frac{S_{light} I_{ph}}{S_{sensor} P} \quad (1)$$

where S_{light} represents the light spot area (9 mm^2) of 785 nm laser, S_{sensor} represents the sensor area (around $256.03 \text{ } \mu\text{m}^2$), P is the laser power and I_{ph} ($I_{ph} = I_{illumination} - I_{dark}$) is the photocurrent. The relationship between P and R under various biases is shown in Figure 3e. At $V_{sd} = -5 \text{ V}$, R drastically increases from 0.61 A W^{-1} to the maximum of 7.47 A W^{-1} as P decrease from 110 to 0.1 mW . When $P = 0.1 \text{ mW}$, R is greatly improved from 1.65 to 7.47 A W^{-1} as V_{sd} increase from -1 to -5 V , which can be attributed to the increase of I_{ph} . These results indicate the high photoelectric response of the multilayer InSe photodetector.

Specific detectivity (D^*) is another key parameter that reflects the sensitivity of photodetectors. That is, when the detector area is 1 cm^2 and the bandwidth is 1 Hz , the signal-to-noise ratio per unit of power can be given. D^* is limited by three kinds of noise: thermal fluctuation noise, Johnson noise, and shot noise from dark current. In this study, shot noise is the major among all of the noise. Here in this study, D^* can be given by^[50]

$$D^* = \frac{R}{\sqrt{2qI_{\text{dark}}}} \quad (2)$$

where q is the quantity of electron charge ($1.602 \times 10^{-19} \text{ C}$). Figure 3f shows the figure of D^* as a function of V_{sd} under 0.1 mW laser. Similar to the trends of R , when V_{sd} decreases from -5 to -2 V , D^* value accordingly decreases from a maximum of 4.56×10^{13} to 3.30×10^{13} Jones. However, the value of D^* no longer drops after V_{sd} is less than -2 V , and tends to be stable as V_{sd} decreases. Due to the large photocurrent and responsivity under large V_{sd} , the multilayer InSe detector can exhibit strong weak signal detection capabilities. However, when V_{sd} is less than -2 V , the shot noise inside the multilayer InSe detector has a relatively large impact, which limits the performance of the multilayer indium selenide. Nevertheless, the R and D^* of the multilayer InSe photodetector are still better than some previously reported photodetectors based on InSe or other TMD materials, which proves that the multilayer InSe is an excellent material for photodetectors.

Figure 4a shows the optical image of our device, where the yellow lines are the Au/Ti electrodes and the purple part is the SiO_2 substrate. The blue part is the multilayer InSe sheets with high surface quality and a large sensing area. Subsequently, we processed further experiments on this device to verify that multilayer InSe is the main contribution of

polarized light-sensitive photocurrent. The photodetector is placed in a 2D movement platform which enables us to scan the photocurrent of each point of multilayer InSe, the range of scanning area is set to $52 \times 50 \mu\text{m}$, and the step distance is $1 \mu\text{m}$. A 785 nm laser with a power of 0.2 mW is used and the bias is -2 V . As shown in Figure 4b–f, the photocurrent mapping of multilayer InSe photocurrent shows surprising results. Here, the black dotted line in the figure represents the outline of the multilayer InSe and the white lines represent the gold electrodes. It can be seen that all the points of InSe exhibit obvious photo-response, not just the points that are near the sensing area, which proves that multilayer InSe has photoelectric conversion ability. Here, the polarization angle is set to be 0° when the photocurrent reduces to the minimum, which means it is along the armchair direction. The photocurrent of multilayer InSe changes uniformly along with the polarization angle, when the polarization angle increases to 90° , the photocurrent of the multilayer InSe increases to the maximum, because the polarization angle is along the zigzag direction. Therefore, the polarization-sensitive photocurrent mainly comes from the different electron transition rates caused by the anisotropy of γ -InSe crystal structure, rather than the position relationship between electrode and sensing material. It can be seen that multilayer γ -InSe as an entirety shows excellent and uniform sensitivity to polarized light. As a polarized light photodetector, multilayer InSe has a large effective sensing area and outstanding capacity to detect a subtle change in polarized light, which has great technical advantages and a promising future.

To further verify the performance of the multilayer InSe photodetector, the response speed is measured by the use of a signal generator and oscilloscope. As shown in Figure 5a, the green line represents the 785 nm laser signal with a square wave of 100 Hz switching between ON and OFF status, and the blue line

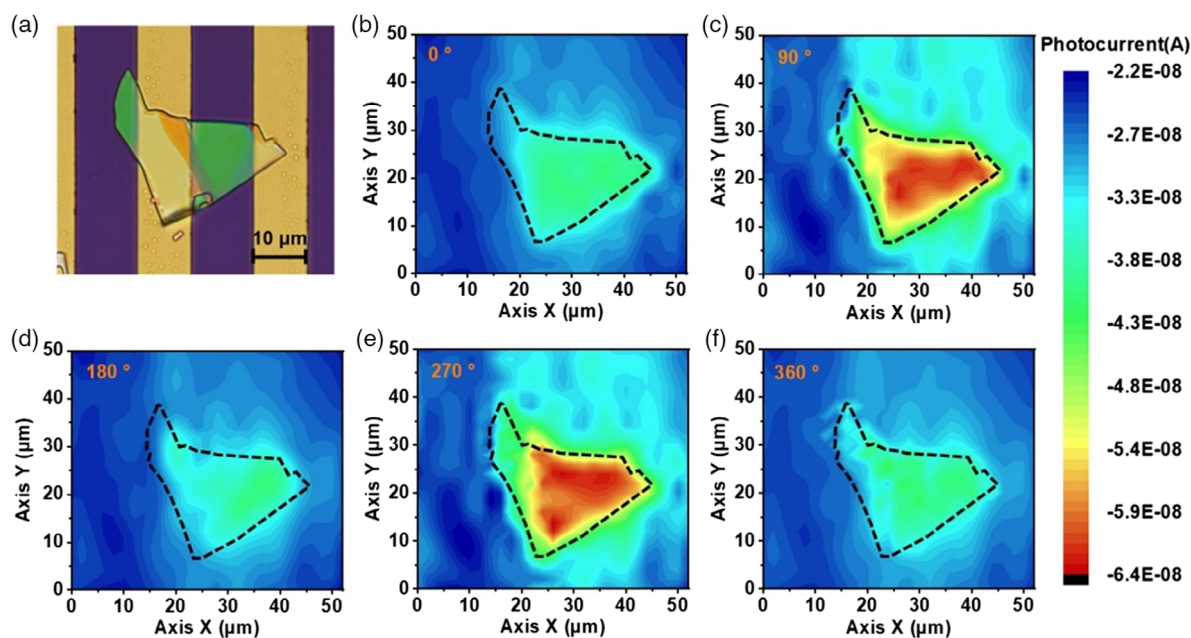


Figure 4. a) 50 times magnified optical image of multilayer InSe photodetector. b–f) With the area of $52 \times 50 \mu\text{m}$, the mapping diagram of photoelectric response of InSe photodetector under polarized light with the power of 0.2 mW .

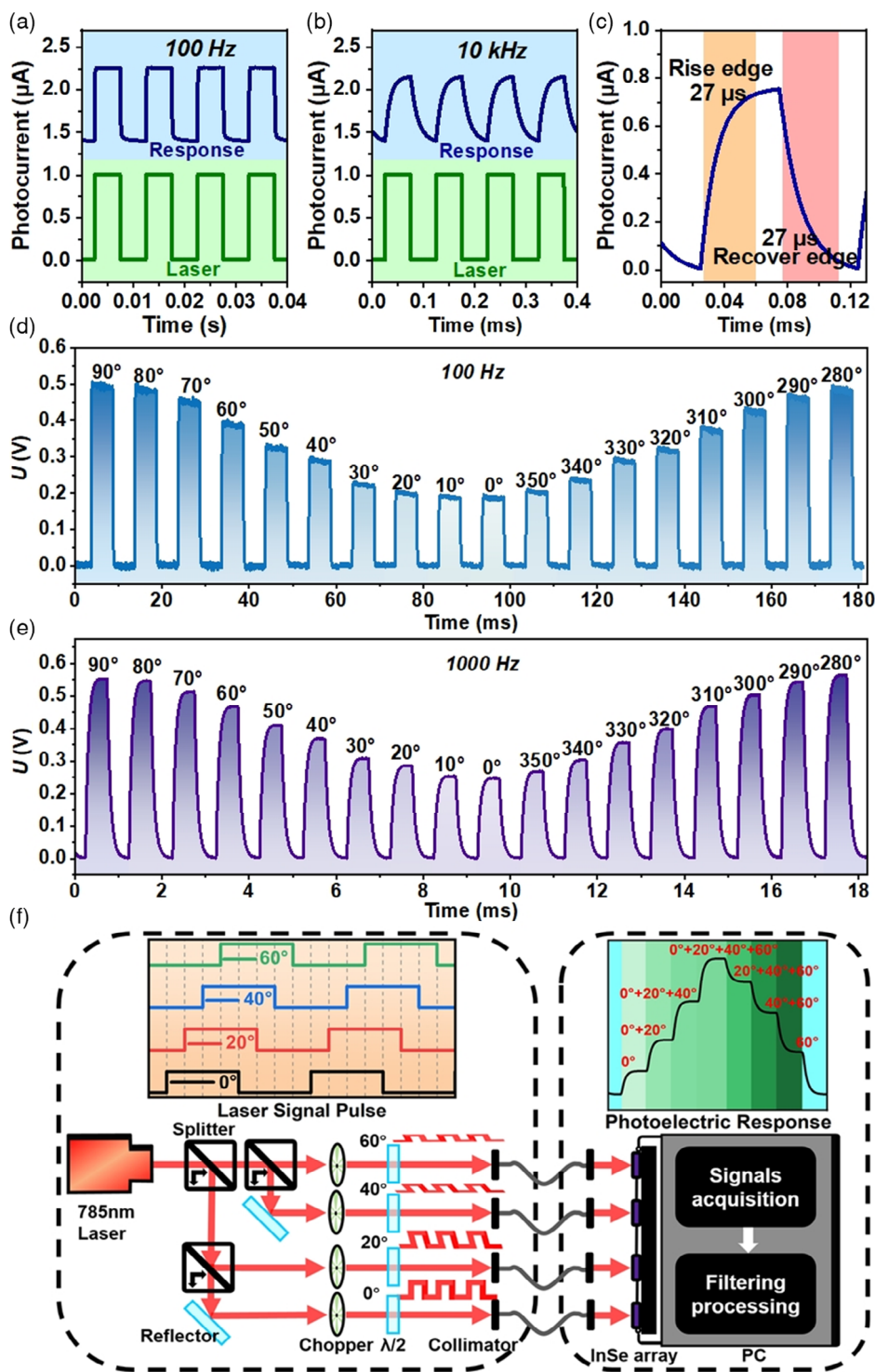


Figure 5. a,b) Reproducible on/off switching of the photocurrent under irradiation of 785 nm laser with frequency of 100 and 10 kHz, respectively. c) Single photoelectric response of InSe photodetector under 10 kHz laser, showing the ability to detect high-frequency signals. d,e) The photoelectric response of InSe photodetector to laser with polarization angles from 0 to 180° at signal frequencies of 100 and 1000 Hz, respectively. f) Schematic diagram of multilayer γ -InSe polarized light detector applied in polarized optical communication.

represents the photoelectric response. The multilayer InSe photodetector exhibits outstanding repeatability and stable response. As shown in Figure 5b, the photoelectric response remains stable even though the laser signal frequency is raised to 10 kHz. The rising time (τ_r) is defined as the time for photocurrent increase from 10% to 90% of maximum, and the falling time (τ_f) is defined to describe the recovery of photocurrent similarly. A single cycle of rising and falling response is shown in Figure 5c, τ_r and τ_f are both around 27 μ s. The short photoelectric response time of this photodetector is mainly due to the ultrafast carrier mobility. When the electron is excited by the laser, under the attraction of external bias, the electrons and holes are separated rapidly, and the electrons can transit rapidly along the atoms in InSe. What's more, we compare the performance of other studies based on InSe (See Figure S4, Supporting Information): black phosphorous/InSe,^[41] graphene/InSe/MoS₂,^[42] InSe with graphene electrodes,^[51] 1D Se-2D InSe,^[52] Few-layered InSe,^[53] AsP/InSe,^[54] wafer-scale InSe,^[40] atomic layers InSe.^[39] The performance of the multilayer γ -InSe photodetector is marked in red dash line square, high responsivity of 7.47 A W⁻¹ and fast response time of 27 μ s can be achieved simultaneously. The outstanding performance indicates the great potential of multilayer InSe photodetector in optical sensing and imaging.

As shown in Figure 5d,e, the polarized depended response time of multilayer γ -InSe under laser at a frequency of 100 and 1000 Hz are measured, respectively. When laser frequency is 100 Hz, as the polarization angle change, the intensity of photoelectric response change accordingly. It can be seen that the multilayer InSe polarized detector can rapidly follow the change of laser signal. Surprisingly, when the laser frequency is increased to 1000 Hz, the response time of this photodetector under all polarization angles is extremely close, which means it is not sensitive to the laser polarization angle. When the laser polarization angle is 0° (Armchair direction) and 90° (Zigzag direction), the response time is 26.9 and 27.1 μ s, respectively. For photodetectors, the stability of response time is essential for signal acquisition and processing. If the response time changes greatly along with the polarized light, it is not conducive to signal acquisition and is prone to large errors.

From the aforementioned measurement and analysis, photo-detection performance and outstanding sensitivity of multilayer γ -InSe photodetector have been proved. Based on these studies, further study about the PDM application of this photodetector is explored. Recently, with the emergence of wireless electronic products, faster and more stable communication speed has become an important selling point of products, and optical communication has attracted extensive interest because it can large amount of information at ultrafast transmission speed. By modulating multiple laser beams with different polarization states, more data can be transmitted without increasing the frequency spectrum. In the current research, although the modulation of signal laser has been achieved, how to use a high-performance polarization detector to achieve stable and reliable demultiplexing is still a problem. The test system is shown in the Figure 5e, the origin laser is generated by a 785 nm laser source, then it is divided into four laser beams through a beam splitter and the intensity remains unchanged. The two laser beams will first pass the half-wave plates with angles of 0°, 20°, 40°, and 60°, and then the choppers with the same frequency but different phases. With

the optical fiber, the encoded laser signal can be transmitted over a long distance and then irradiated on the InSe photodetector array, respectively. By the sensitivity of the indium selenide polarized light detector to different polarization angles, response signals with different intensities can be generated. After signal processing by the computer, the information in the coded laser can be read. When using the polarized light detector in this study, multilayer InSe can not only sensitively detect the change of polarization angle, but also stably and accurately capture high-frequency polarized laser signal, which indicates the potential in PDM application.

3. Conclusion

In this study, high-quality multilayer γ -InSe is prepared by mechanical exfoliation. By studying the PL spectrum of multilayer indium selenide, it is found that its sensitivity to polarized light comes from its internal crystal structure. The PL intensity of multilayer InSe is highly sensitive to the polarization angles and exhibits an anisotropic ratio of 1.53. The period of PL intensity is consistent with the included angle of the armchair and zigzag directions of the InSe crystal, which indicates the intrinsic anisotropy of electron transition. What's more, the multilayer InSe photodetector exhibits excellent photodetection capability with a responsivity of up to 7.47 A W⁻¹ and specific detectivity of 4.56×10^{13} Jones under 785 nm laser illumination. Moreover, a fast response time of 27 μ s can be achieved simultaneously. Most important of all, the photocurrent of multilayer InSe photodetector also shows outstanding sensitivity to polarization angle of laser and the anisotropic ratio of this device reaches 2.7, which indicates the impressive polarization detection ability. In addition, in the photoelectric mapping measurement, it is found that the multilayer InSe photodetector has a large effective detection area, and every point on the sensor exhibits high sensitivity. In the study of multilayer InSe, the principle of polarized light detection of it has been explored, and the ability of multilayer InSe photodetector in polarized light detection has been brought into full play. Since the response time of this device is not sensitive to the polarization angle, it can maintain a fast and stable response time at every polarization angle showing its potential PDM application in the field of polarized light communication.

4. Experimental Section

Device Fabrication: Here in this study, the undoped γ -InSe crystal was prepared by the Bridgman growth method. The multilayer InSe was prepared through mechanical exfoliation (See Figure S5, Supporting Information). Using an adhesive tape, the multilayer InSe film was stripped off from crystal materials and gradually thinned through several stripping. Later, the multilayer InSe was transferred onto the top of the SiO₂ substrate. For observation of surface morphology and selection of multilayer InSe, the optical image of it can be obtained by high magnification optical microscopy (Nikon ECLIPSE LV150N). To fabricate the multilayer InSe polarization photodetector, the source and drain electrodes were needed to contact the two sides of the multilayer InSe. By the use of electron beam lithography (EBL, Raith BV EBPG 5150), the pattern of the electrodes was developed on the photoresist. Subsequently, the vacuum evaporation coating system was used for the deposition of metal electrodes. Firstly, a 5 nm layer of titanium was deposited on the substrate

to enhance the mechanical strength of the electrodes. Then, in the main part of electrodes, a 40 nm layer of Au was deposited onto the titanium layer. Finally, the partially prepared device was soaked into the acetone solution for 10 min to remove the unnecessary photoresist and the multilayer InSe polarization photodetector is fabricated.

Measurements and equipment: To verify the phase of the prepared InSe nanofilm, Raman spectroscopy (LabRAM HR Evolution) was used. To observe the surface quality of multilayer γ -InSe photodetectors and measure the thickness of the multilayer film, AFM (Bruker Dimension Icon) was used. Furthermore, the PL spectrum was used to analyze the intrinsic anisotropy of multilayer InSe, it is measured by a high-resolution spectrograph platform (Andor Shamrock 500i). Here in this study, the 588 and 785 nm lasers were used as the linear polarized light source. By rotating the 1/2 waveplate, the polarization angle of the laser can be changed. The *I*-*V* curves and photocurrent of the multilayer InSe photodetector were studied by a probe station (Lakeshore TTPX) and a semiconductor characterization system (Keithley 4200-SCS). For measurement of photoelectric response time, a signal generator (Keysight 33600A) generated a square wave laser signal, and the photoresponse signal was detected by the oscilloscope (Keysight DSOX3104T).

Band structure calculation: In this study, DFT was employed to study the electronic structure of multilayer γ -InSe, as implemented in Vienna Ab initio Simulation Package (VASP). Generalized gradient approximation (GGA) with a Perdew–Burke–Ernzerhof (PBE) functional was treated as the exchange–correlation energy. An additional $U = 2$ eV was added to the In4d electrons to describe the strong correlation effect. To better describe the van der Waals interaction, the Tkatchenko–Scheffler method is used. Here, the cut-off energy was 400 eV and the Gamma-centered *k*-point grid was set as $20 \times 20 \times 1$. The full relaxation for the overall system was allowed to find the ground state through computing the Hellmann–Feynman forces within total energy and force convergences of 10^{-6} eV and 2×10^{-1} eV Å⁻¹. The self-consistency threshold of total energy was set at 10^{-6} eV.

Supporting Information

Supporting Information is available from the Wiley Online Library or from the author.

Acknowledgements

X.W. and B.W. contributed equally to this work. The authors gratefully acknowledge the financial support from the National Natural Science Foundation (No. 62104155) of China, NSF of Guangdong province (No. 2022A1515011667), and Shenzhen Science and Technology Innovation Commission (No. RCJC20200714114435063). The authors wish to acknowledge the assistance on TEM/FIB received from the Electron Microscope Center of Shenzhen University.

Conflict of Interest

The authors declare no conflict of interest.

Data Availability Statement

Research data are not shared.

Keywords

anisotropic photoluminescence (PL) spectrum, multilayer γ -InSe, polarization detection, polarization-dependent photocurrent

Received: April 23, 2022

Revised: July 11, 2022

Published online: August 17, 2022

- [1] Y. D. Cui, F. F. Lu, X. M. Liu, *Sci. Rep.* **2017**, 7, 9.
- [2] Y. M. Giraldo, K. J. Leitch, I. G. Ros, T. L. Warren, P. T. Weir, M. H. Dickinson, *Curr. Biol.* **2018**, 28, 2845.
- [3] S. X. Li, G. P. Zhang, H. Xia, Y. S. Xu, C. Lv, H. B. Sun, *Nanoscale* **2019**, 11, 18272.
- [4] J. R. Petriglieri, C. Laporte-Magoni, P. Gunkel-Grillon, M. Tribaudino, D. Bersani, O. Sala, M. Le Mestre, R. Vigliaturo, N. B. Gandolfi, E. Salvioli-Mariani, *Geosci. Front.* **2020**, 11, 189.
- [5] S. B. Powell, R. Garnett, J. Marshall, C. Rizk, V. Gruev, *Sci. Adv.* **2018**, 4, 8.
- [6] L. Tong, X. Y. Huang, P. Wang, L. Ye, M. Peng, L. C. An, Q. D. Sun, Y. Zhang, G. M. Yang, Z. Li, F. Zhong, F. Wang, Y. X. Wang, M. Motlag, W. Z. Wu, G. J. Cheng, W. D. Hu, *Nat. Commun.* **2020**, 11, 10.
- [7] B. H. Tu, J. Hong, P. P. Yao, B. H. Meng, Y. L. Yuan, M. M. Zhang, J. W. Weng, *Acta Opt. Sin.* **2020**, 40, 13.
- [8] H. J. Zhao, W. J. Xu, Y. Zhang, X. D. Li, H. Zhang, J. B. Xuan, B. Jia, *Opt. Express* **2018**, 26, 28589.
- [9] Z. Q. Zhou, Y. Cui, P. H. Tan, X. L. Liu, Z. M. Wei, *J. Semicond.* **2019**, 40, 11.
- [10] C. X. Cong, J. Z. Shang, Y. L. Wang, T. Yu, *Adv. Opt. Mater.* **2018**, 6, 15.
- [11] W. H. Wu, Q. Zhang, X. Zhou, L. Li, J. W. Su, F. K. Wang, T. Y. Zhai, *Nano Energy* **2018**, 51, 45.
- [12] J. D. Yao, Z. Q. Zheng, G. W. Yang, *Adv. Funct. Mater.* **2017**, 27, 10.
- [13] L. Ye, P. Wang, W. J. Luo, F. Gong, L. Liao, T. D. Liu, L. Tong, J. F. Zang, J. B. Xu, W. D. Hu, *Nano Energy* **2017**, 37, 53.
- [14] X. Zhou, X. Z. Hu, J. Yu, S. Y. Liu, Z. W. Shu, Q. Zhang, H. Q. Li, Y. Ma, H. Xu, T. Y. Zhai, *Adv. Funct. Mater.* **2018**, 28, 28.
- [15] S. Pal, A. Verma, Y. K. Prajapati, J. P. Saini, *Opt. Quantum Electron.* **2017**, 49, 13.
- [16] J. Wang, Y. N. Jiang, Z. R. Hu, *Opt. Express* **2017**, 25, 22149.
- [17] C. Xing, J. H. Zhang, J. Y. Jing, J. Z. Li, F. Shi, *Chem. Eng. J.* **2019**, 370, 120.
- [18] D. W. He, Y. L. Wang, Y. Huang, Y. Shi, X. R. Wang, X. F. Duan, *Nano Lett.* **2019**, 19, 331.
- [19] Q. Li, Y. H. Zhao, J. Y. Guo, Q. H. Zhou, Q. Chen, J. L. Wang, *Nanoscale* **2018**, 10, 3799.
- [20] H. Liu, J. T. Sun, C. Cheng, F. Liu, S. Meng, *Phys. Rev. Lett.* **2018**, 120, 6.
- [21] X. Tang, H. Chen, J. S. Ponraj, S. C. Dhanabalan, Q. L. Xiao, D. Y. Fan, H. Zhang, *Adv. Sci.* **2018**, 5, 9.
- [22] D. A. Chenet, O. B. Aslan, P. Y. Huang, C. Fan, A. M. van der Zande, T. F. Heinz, J. C. Hone, *Nano Lett.* **2015**, 15, 5667.
- [23] A. T. Hanbicki, H. J. Chuang, M. R. Rosenberger, C. S. Hellberg, S. V. Sivaram, K. M. McCreary, I. I. Mazin, B. T. Jonker, *ACS Nano* **2018**, 12, 4719.
- [24] L. Tong, X. Y. Duan, L. Y. Song, T. D. Liu, L. Ye, X. Y. Huang, P. Wang, Y. H. Sun, X. He, L. J. Zhang, K. Xu, W. D. Hu, J. B. Xu, J. F. Zang, G. J. Cheng, *Appl. Mater. Today* **2019**, 15, 203.
- [25] J. Xia, X. L. Wang, B. K. Tay, S. S. Chen, Z. Liu, J. X. Yan, Z. X. Shen, *Nano Res.* **2017**, 10, 1618.
- [26] Y. Xin, X. X. Wang, Z. Chen, D. Weller, Y. Y. Wang, L. J. Shi, X. Ma, C. J. Ding, W. Li, S. Guo, R. B. Liu, *ACS Appl. Mater. Interfaces* **2020**, 12, 15406.
- [27] D. Kufer, G. Konstantatos, *ACS Photonics* **2016**, 3, 2197.
- [28] X. F. Song, X. H. Liu, D. J. Yu, C. X. Huo, J. P. Ji, X. M. Li, S. L. Zhang, Y. S. Zou, G. Y. Zhu, Y. J. Wang, M. Z. Wu, A. Xie, H. B. Zeng, *ACS Appl. Mater. Interfaces* **2018**, 10, 2801.
- [29] J. Zhang, Y. T. Liu, X. L. Zhang, Z. Y. Ma, J. Li, C. Zhang, A. Shaikenova, B. Renat, B. D. Liu, *ChemistrySelect* **2020**, 5, 3438.

- [30] D. A. Bandurin, A. V. Tyurnina, G. L. Yu, A. Mishchenko, V. Zolyomi, S. V. Morozov, R. K. Kumar, R. V. Gorbachev, Z. R. Kudrynskiy, S. Pezzini, Z. D. Kovalyuk, U. Zeitler, K. S. Novoselov, A. Patane, L. Eaves, I. V. Grigorieva, V. I. Fal'ko, A. K. Geim, Y. Cao, *Nat. Nanotechnol.* **2017**, 12, 223.
- [31] L. D. Chen, H. Miao, T. X. Han, J. Feng, E. Z. Liu, Y. F. Cheng, J. L. Mu, J. Fan, X. Y. Hu, *J. Phys. D-Appl. Phys.* **2018**, 51, 6.
- [32] A. I. Dmitriev, V. V. Vishnjak, G. V. Lashkarev, V. L. Karbovskiy, Z. D. Kovaljuk, A. P. Bahtinov, *Phys. Solid State* **2011**, 53, 622.
- [33] P. H. Ho, Y. R. Chang, Y. C. Chu, M. K. Li, C. A. Tsai, W. H. Wang, C. H. Ho, C. W. Chen, P. W. Chiu, *ACS Nano* **2017**, 11, 7362.
- [34] G. W. Mudd, S. A. Svatek, T. Ren, A. Patane, O. Makarovskiy, L. Eaves, P. H. Beton, Z. D. Kovalyuk, G. V. Lashkarev, Z. R. Kudrynskiy, A. I. Dmitriev, *Adv. Mater.* **2013**, 25, 5714.
- [35] H. Y. Nan, S. J. Guo, S. Cai, Z. R. Chen, A. Zafar, X. M. Zhang, X. F. Gu, S. Q. Xiao, Z. H. Ni, *Semicond. Sci. Technol.* **2018**, 33, 7.
- [36] M. Teena, A. G. Kunjomana, K. Ramesh, R. Venkatesh, N. Naresh, *Sol. Energy Mater. Sol. Cells* **2017**, 166, 190.
- [37] M. J. Hamer, J. Zultak, A. V. Tyurnina, V. Zolyomi, D. Terry, A. Barinov, A. Garner, J. Donoghue, A. P. Rooney, V. Kandyba, A. Giampietri, A. Graham, N. Teutsch, X. Xia, M. Koperski, S. J. Haigh, V. I. Fal'ko, R. V. Gorbachev, N. R. Wilson, *ACS Nano* **2019**, 13, 2136.
- [38] T. V. Shubina, W. Desrat, M. Moret, A. Tiberj, O. Briot, V. Y. Davydov, A. V. Platonov, M. A. Semina, B. Gil, *Nat. Commun.* **2019**, 10, 8.
- [39] S. D. Lei, L. H. Ge, S. Najmaei, A. George, R. Kappera, J. Lou, M. Chhowalla, H. Yamaguchi, G. Gupta, R. Vajtai, A. D. Mohite, P. M. Ajayan, *ACS Nano* **2014**, 8, 1263.
- [40] Z. B. Yang, W. J. Jie, C. H. Mak, S. H. Lin, H. H. Lin, X. F. Yang, F. Yan, S. P. Lau, J. H. Hao, *ACS Nano* **2017**, 11, 4225.
- [41] R. Cao, H. D. Wang, Z. N. Guo, D. K. Sang, L. Y. Zhang, Q. L. Xiao, Y. P. Zhang, D. Y. Fan, J. Q. Li, H. Zhang, *Adv. Opt. Mater.* **2019**, 7, 7.
- [42] Z. S. Chen, Z. L. Zhang, J. Biscaras, A. Shukla, *J. Mater. Chem. C* **2018**, 6, 12407.
- [43] S. Y. Gao, L. Liu, B. Wen, X. Zhang, *Phys. Chem. Chem. Phys.* **2021**, 23, 6075.
- [44] T. Zheng, Z. T. Wu, H. Y. Nan, Y. F. Yu, A. Zafar, Z. Z. Yan, J. P. Lu, Z. H. Ni, *RSC Adv.* **2017**, 7, 54964.
- [45] Y. Li, T. M. Wang, M. Wu, T. Cao, Y. W. Chen, R. Sankar, R. K. Ulaganathan, F. C. Chou, C. Wetzel, C. Y. Xu, S. G. Louie, S. F. Shi, *2D Mater.* **2018**, 5, 9.
- [46] Y. Li, T. M. Wang, H. Wang, Z. P. Li, Y. W. Chen, D. West, R. Sankar, R. K. Ulaganathan, F. C. Chou, C. Wetzel, C. Y. Xu, S. B. Zhang, S. F. Shi, *Nano Lett.* **2018**, 18, 5078.
- [47] S. Chen, R. Cao, X. Chen, Q. Wu, Y. H. Zeng, S. Gao, Z. N. Guo, J. L. Zhao, M. Zhang, H. Zhang, *Adv. Mater. Interfaces* **2020**, 7, 8.
- [48] Y. Ge, M. J. Zhang, L. Wang, L. H. Meng, J. L. Tang, Y. Chen, L. X. Wang, H. Z. Zhong, *Adv. Opt. Mater.* **2019**, 7, 7.
- [49] X. Zhou, X. Z. Hu, B. Jin, J. Yu, K. L. Liu, H. Q. Li, T. Y. Zhai, *Adv. Sci.* **2018**, 5, 9.
- [50] X. Gong, M. H. Tong, Y. J. Xia, W. Z. Cai, J. S. Moon, Y. Cao, G. Yu, C. L. Shieh, B. Nilsson, A. J. Heeger, *Science* **2009**, 325, 1665.
- [51] W. G. Luo, Y. F. Cao, P. G. Hu, K. M. Cai, Q. Feng, F. G. Yan, T. F. Yan, X. H. Zhang, K. Y. Wang, *Adv. Opt. Mater.* **2015**, 3, 1418.
- [52] H. M. Shang, H. Y. Chen, M. J. Dai, Y. X. Hu, F. Gao, H. H. Yang, B. Xu, S. C. Zhang, B. Y. Tan, X. Zhang, P. A. Hu, *Nanoscale Horiz.* **2020**, 5, 564.
- [53] S. R. Tamalampudi, Y. Y. Lu, U. R. Kumar, R. Sankar, C. D. Liao, B. K. Moorthy, C. H. Cheng, F. C. Chou, Y. T. Chen, *Nano Lett.* **2014**, 14, 2800.
- [54] F. Wu, H. Xia, H. D. Sun, J. W. Zhang, F. Gong, Z. Wang, L. Chen, P. Wang, M. S. Long, X. Wu, J. L. Wang, W. C. Ren, X. S. Chen, W. Lu, W. D. Hu, *Adv. Funct. Mater.* **2019**, 29, 9.